Soft Matter

Gallium Oxide-Stabilized Oil in Liquid Metal Emulsions

SCHOLARONE™
Manuscripts

Gallium Oxide-Stabilized Oil in Liquid Metal Emulsions

Najam Ul Hassan Shah,[a] Wilson Kong, [a] Nathan Casey, [a] Shreyas Kanetkar, [a] Robert Y. Wang, [a] and Konrad Rykaczewski*[a]*

a) School for Engineering of Matter, Transport and Energy
Arizona State University
Tempe, AZ, 85287, USA
*E-mail: rywang@asu.edu, konradr@asu.edu

Abstract

Gallium based liquid metals (LM) have prospective biomedical, stretchable electronics, soft robotics, and energy storage applications, and are being widely adopted as thermal interface materials. The danger of gallium corroding most metals used in microelectronics requires the cumbersome addition of "barrier" layers or LM break-up into droplets within an inert matrix such as silicone oil. Such LM-in-oil emulsions are stabilized by native oxide on the droplets but have decreased thermal performance. Here we show that mixing of the silicone oil into an LM-air foam yields emulsions with inverted phases. We investigate the stability of these oil-in-LM emulsions through a range of processing times and oil viscosities, and characterize the impact of these parameters on the materials' structure and thermal property relationships. We demonstrate that the emulsion with 40 vol% of 10 cSt silicone oil provides a unique thermal management material with a 10 Wm^{-1}K^{-1} thermal conductivity and an exterior lubricant thin film that completely prevents corrosion of contacting aluminum.

Introduction

The tagline "coming soon to electronics near you" could be used to express the recent rush to adopt liquid metals (LM) or their foamed versions as thermal interface materials (TIMs) in the integrated electronics' industry.[1,2] These soft, conductive materials also have prospective biomedical, stretchable electronics, soft robotics, electromagnetic shielding, and energy storage applications.[2–9] However, thermal management of microelectronics is currently by far the most wide spread and impactful use of LMs.[1,10,11] For this application, the primary advantage of these gallium-based room temperature LMs and their foams is that their thermal conductivity (10 to 25 $Wm^{-1}K^{-1}$) is much greater than that of traditional fluid TIMs such as composite silicone greases (1 to 4 $Wm^{-1}K^{-1}$).[12] The primary disadvantages of using LMs are gallium-induced alloying, corrosion, or embrittlement of most metals used in electronics.[13–16] Aside from expensive packaging-level approaches such as introduction of corrosion barrier films[17,18] (which also allow LM connection with microelectronic leads[19,20]), the corrosion issues are most commonly addressed by dispersing the LM as microdroplets in matrix materials such as silicones to form "LM-in-oil" emulsions or soft solid composites.[21–25] The resulting disruption of the metal phase decreases the thermal conductivity of these emulsions to typical 1 to 5 $Wm^{-1}K^{-1}$ level. Here we show that inversion of the liquid metal and silicone oil phases (*i.e.*, making "oil-in-LM" emulsions) enabled by prior foaming of the LM can resolve the corrosion issue while still providing a high thermal performance.

While dispersing LM into another fluid medium is relatively simple, the opposite is more challenging owing to LM's high density and surface tension as well as immiscibility with other liquids.[26] When one immiscible liquid more favorably emulsifies into another liquid, such as LM into silicone oil, inverting this emulsion orientation typically requires the introduction of

emulsifying agents or surfactants.[27,28] Figure 1a shows that after dispersion in silicone oil or other liquid, the LM micro-droplets are prevented from coalescing through rapidly forming native gallium oxide shells.[6,29] This oxide layer has surfactant-like qualities including augmentation of the liquid metal's surface tension.[30,31] During stirring of the bulk LM in air, the growth of this oxide on the LM-air interface and subsequent incorporation of its fragments into the liquid enables the formation of LM-based foams with stable air bubbles.[32–36] While these LM foams containing air or another gaseous species are rapidly gaining attention, methods of effectively incorporating an immiscible liquid phase into LM is largely unknown.

In this work, we demonstrate that stable "oil-in-LM" emulsions can be created through the incorporation of silicone oil (SO) into LM-based foam (see Figure 1). These emulsions are achieved through simple shear mixing in air without any specialized processing techniques. We systematically characterize the impact of oil viscosity, which strongly influences formation of LM-in-oil emulsions, on the dynamics of oil-in-LM emulsion fabrication and phase inversion characteristics. Additionally, we examine how the volumetric content of SO impacts its internalization in the foam, effects the emulsion's thermal conductivity, and inhibits corrosion on aluminum substrates. We show that the introduced oil-in-LM emulsions serve to address the intrinsic flaws of LM-based TIMs, as they can hinder aluminum corrosion due to their lubricant impregnated surface while also exhibiting a high thermal conductivity.
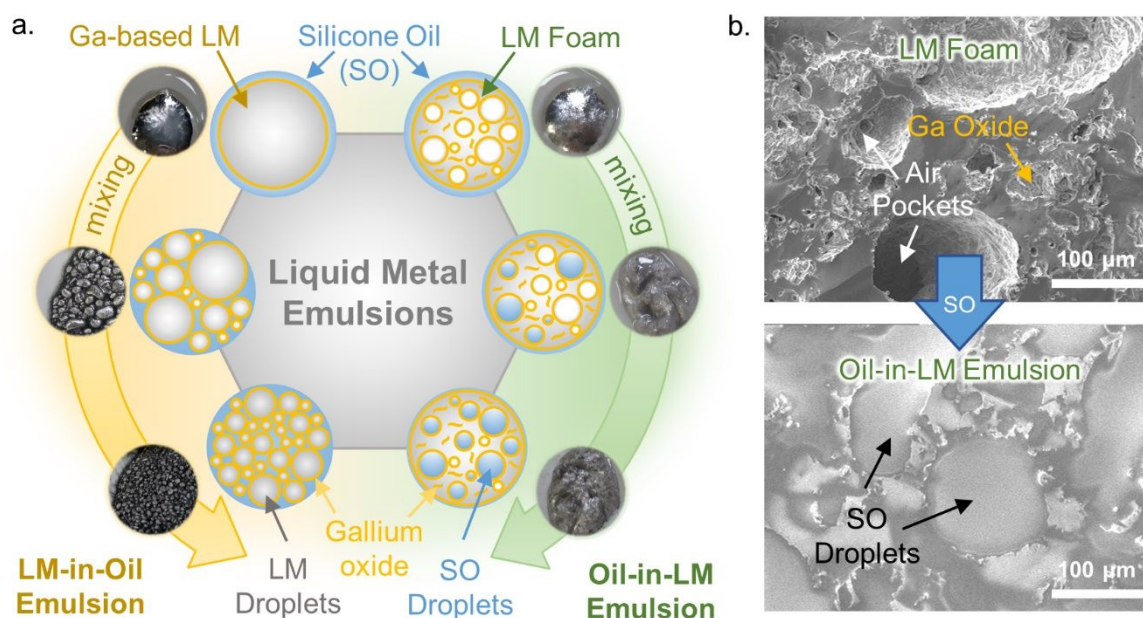
Figure 1 (a) Overview of shear-mixing based fabrication of LM-in-oil emulsions and oil-in-LM emulsions and (b) cross-sectional SEM images of LM-based foam before and after mixing with silicone oil (SO) which results in the formation of oil-in-LM emulsion.

Results and Discussion

The mixing of melted gallium with SO leads to formation of the LM droplets whose size depends on the viscosity of the oil as well as the mixing rate and time. Figure 2a shows images of LM-in-oil emulsions formed by 30 minutes of manually mixing 10, 100, 1000, and 10,000 cSt SOs into LM at a 20:80 volume ratio. In the 10 cSt SO, the LM separates into a widely distributed mix of large droplet sizes (greater than 1 mm) and smaller sizes. Since the shear stress that leads to droplet breakup scales with the viscosity, the average LM droplet size distribution becomes smaller for higher viscosity oils.[37,38] For example, within 30 minutes of mixing in the 10,000 cSt SO, the droplet size is reduced to tens of microns or smaller (droplet size distribution for all the oil viscosities and three mixing times are available in Supplemental Electronic Information). While the oil viscosity does not impact the effective thermal conductivity of the LM-in-oil emulsions

under mild compression (~2 mm thick samples under 0.1 MPa pressure have values under 2 Wm⁻¹K⁻¹ that match our prior results for silicone pads with LM droplets[39]), it does have a strong influence on the dynamics of formation of emulsions with inverted phases.

The generation and incorporation of oxide flakes and oxide-covered air bubbles into LM is necessary to form oil-in-LM emulsions. Prior to addition of the SO, we generated the LM foam through 2 hours of rapid shear mixing of melted gallium at 600 rpm in an air environment.[33] This material contains a mixture of wrinkled gallium oxide flakes, oxide-covered air bubbles, and occasional air pores with sizes ranging from a tenth to hundreds of micrometers[33] (see also Figure 1b). With these internal features, SO readily mixes into the foam (at 20:80 SO:LM foam volume ratio) within several minutes of manual shear mixing of the two liquids at about 120 rpm. The cross-sectional electron micrographs in Figures 1b and optical images in Figure 2b clearly show that much of the SO disperses into distinct droplets surrounded by the continuous LM phase with the foam features (as shown through the glossy reflections on the cross sectioned surfaces). Since the SO contains dissolved air, the oil droplets are likely covered by a gallium oxide shell. Using this approach we can create oil-in-LM emulsions with silicones with viscosity ranging from 10 to 10,000 cSt. However, extended stirring of the created oil-in-LM emulsions produces vastly different outcomes that depend on the used oil viscosity. Specifically, the schematic and images in Figure 2c show that continued mixing of the oil-in-LM emulsion containing the 10,000 cSt SO results in gradual break-up of the emulsion into smaller regions separated by oil and eventual phase inversion into an LM-in-oil emulsion. The illustrative processing map in Figure 2d shows that for the specific case of 20:80 SO:LM foam volume ratio, the decrease in oil viscosity delays or significantly inhibits the onset of this inversion. For example, we did not observe inversion of the phases when using the 10 cSt even after 120 minutes of stirring. It is important to note that this

illustrative processing map is meant to reflect the different phase stability regions and can change based on changes in processing conditions. In addition, the transitions between the phases are gradual, so the boundaries on the processing map are blurred. Next, we investigate how the volumetric content of the SO in these inversion-resistant ("stable") oil-in-LM emulsions impacts their internal structure.
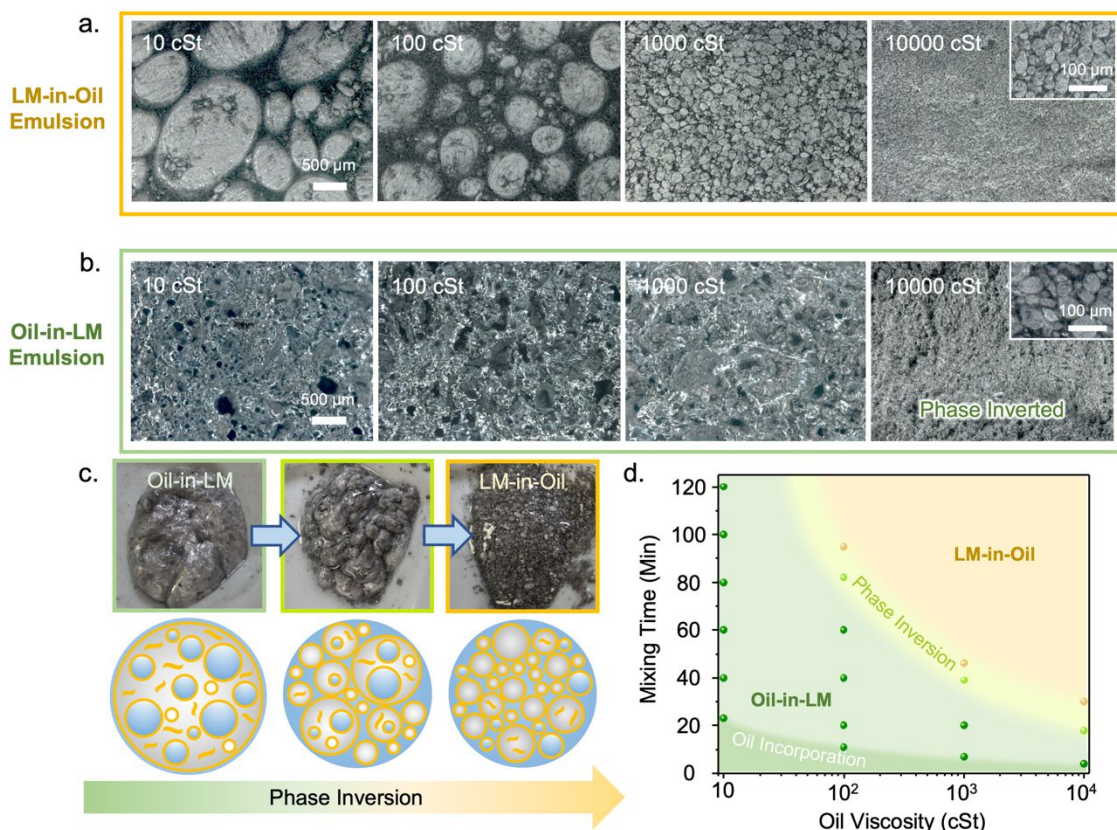
Figure 2. (a) optical images of LM-in-oil emulsions made with 10 to 10,000 cSt viscosity SOs (20:80 SO:LM volume ratio and 30 minutes of mixing), (b) optical images of oil-in-LM emulsion cross sections made with 10 to 10,000 cSt viscosity SOs (20:80 SO:LM foam volume ratio and 30 minutes of mixing), (c) illustrative images and schematics showing potential phase inversion characteristics of oil-in-LM back into LM-in-oil emulsions upon excessive mixing, and (d) illustrative processing map showing the oil-in-LM formation window and phase inversion regions (20:80 SO:LM foam volumetric ratio, 120 rpm manual shear mixing).

Electron micrographs of oil-in-LM emulsions created by 30 minutes of mixing of LM foam with different volume fractions of 10 cSt SO are shown in Figure 3a. The duration for full

internalization of the oil into the foam increased from under 5 minutes to about 30 minutes with increase of the SO:LM foam volumetric ratio from 10:90 to 40:60 (higher ratios are not used in the studies because excess oil outside the emulsion was observed even for longer mixing times). Within the studied range, the increase in the SO mixing content results in corresponding increase in SO pockets observed in the sample cross sections (see Figure 3a). In addition to formation of these closed-cell features, the SO also appears to fill many of the open-cell pores that are produced during the chaotic LM foam fabrication.[33] This dynamic multiscale structure of the starting LM foams also makes it infeasible to provide a more quantitative description of the impact of the oil content and viscosity on the oil-in-LM emulsion structure. However, the large differences in the thermal conductivity of the various emulsions that we describe next implies that such differences in the internal structure could be substantial.

The effective thermal conductivity (k_{eff}) of oil-in-LM emulsions decreases with both the increase in the oil content and its viscosity (see Figure 3b). To provide values relevant to TIM applications, we use the steady-state stepped bar apparatus measurement methodology that reflects the impact of both the intrinsic material property and sample-measurement bar contact resistances (*i.e.*, provides the effective thermal conductivity of the sample, see Experimental Section).[40,41] For LM-based samples, the effect of the thermal resistance is small, so the effective values we report are close to the intrinsic material value.[42] For example, for pure melted gallium we measure 28.7 $\pm$ 1.1 Wm^{-1}K^{-1} that agrees with prior literature value.[43] Incorporation of the oxide flakes, air bubbles, and pores during 120 minutes of stirring the melted gallium at 600 rpm decreases the k_{eff} of the gallium foam to 17.8 $\pm$ 0.7 Wm^{-1}K^{-1} (this value is not impacted by an additional 30 minutes of low speed manual mixing at 120 rpm). When the SO is incorporated into the foam within 30 minutes of mixing, the k_{eff} of the oil-in-LM emulsions experiences a decrease proportional to the

increasing oil volume content (by about 10 Wm^{-1}K^{-1} in the worst case of 40:60 100 cSt SO:LM foam). This result is counterintuitive as the replacement of the low thermal conductivity air ($k =$ 0.024 Wm^{-1}K^{-1}) content with the more conductive SO ($k = 0.2$ to 0.3 Wm^{-1}K^{-1}) should increase the emulsion's thermal conductivity. Since the k_{eff} of the LM foam is not impacted by the additional 30 minutes of mixing without the oil (and the generated oxide and air features), the SO likely does not replace most of the air features (*e.g.*, fill closed air bubbles) but creates additional oil-filled structures. Compared to pure LM or even LM foam, the oil-in-LM emulsions show reductions in effective thermal conductivity. Thus, the addition of these oil-filled structures in combination with air bubble and gallium oxide content appears to disrupt the thermal energy carrier transport through the composite. The increasing oil viscosity likely alters the quantity and size of such features, thereby resulting in a greater decrease of the emulsion's k_{eff}. Despite this decrease, the 9.5 ± 1.1 Wm^{-1}K^{-1} k_{eff} of the SO:LM 40:60 with 10 cSt SO is still multiple times higher than that of typical silicone grease TIMs measured in the same way (1 to 4 Wm^{-1}K^{-1}). Next, we demonstrate that the presence of the oil provides additional anti-corrosive characteristics to the emulsions that make them uniquely suitable for TIMs.
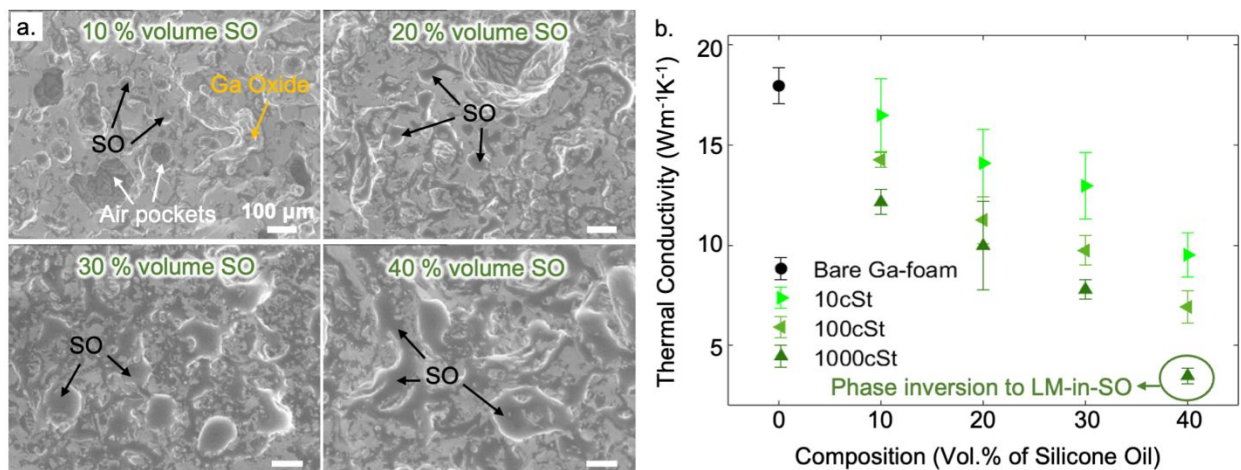
Figure 3. (a) SEM micrographs of oil-in-LM emulsions cross-sections made with 10 cSt viscosity SO with SO:LM foam volumetric ratio ranging from 10:90 to 40:60 (the insets show the corresponding SEM images), and (b) plot of the effective thermal conductivity against the SO volume percentage for oil-in-LM emulsions made with 10 cSt, 100 cSt, and 1000 cSt viscosity of SO.

Generally, the LM embrittlement of aluminum is rapid and takes place within hours of direct contact with the gallium. With sufficient content of the SO, the oil-in-LM emulsions do not embrittle aluminum. We tested this characteristic of the LM foams and emulsions by placing the samples in between two aluminum sheets and applying 0.1 MPa of pressure (the experimental setup was heated to ensure the sample was in the liquid state). The representative images and bar plot in Figure 4a-b show that after 24 hours the LM foams corroded the aluminum foil in all the 20 experimental repetitions. The chance of preventing aluminum embrittlement is dramatically improved with addition of even a small amount of the SO (e.g., by 50% for the 10:90 SO:LM foam composition) and increases nearly linearly with further oil addition. Furthermore, the emulsions with the 40:60 SO:LM foam composition did not corrode aluminum foil in any of the 20 experimental repetitions lasting 24 hours (each exposing the samples to aluminum foil on two sides) or in extended 7-day trials (see Supplemental Information).

The corrosion inhibiting characteristic of the LM-in-oil emulsions likely stems from the presence of a thin SO film on the exterior of the material that provides a barrier between the gallium and aluminum (see schematic in Figure 4c). We confirmed the presence of this exterior SO film by placing small water droplets on the LM foam and on the emulsion with 40:60 SO:LM foam composition. The images in Figure 4d show that the water droplet contact angle increases from about 10º on the LM foam to about 90º on the oil-in-LM emulsion. Since the latter value is in the range of water contact angles typically measured for SO impregnated textured or porous surfaces,[44–46] the exterior surface is likely entirely covered by an oil film. Furthermore, the

presence of the oil meniscus around the perimeter of the water droplet sitting on the oil-in-LM emulsion provides additional evidence of the surface oil film.[47] The oil likely wets the exterior oxide created during the mixing process as well as any new oxide that might be created while applying the emulsion onto the aluminum foil. With about 40% of the emulsion volume occupied by oil, there is an ample supply of it to cover the entire surface prior to contact with a substrate or even during potential volume disruption when making contact (*i.e.*, oil can wick out of pores or leak from ruptured "bubbles" under compression). The presence of the thin oil layer on the surface is also manifested in an increase of the electrical resistance of the emulsions (with about 2 mm thickness and 1 cm^2 area foam samples have resistance below about 1Ω but with addition of the oil this value can be as high as 5 kΩ). Since the same principle of a thin exterior lubricant barrier layer essentially completely protects metal surfaces against a variety of corrosion processes,[48,49] the demonstrated inhibition of aluminum embrittlement by the oil-in-LM emulsion has the potential to also occur in even harsher testing conditions (*e.g.*, elevated temperatures, higher pressures, and during thermomechanical cycling). However, systematic dynamic testing that represents thermomechanical cycling of the samples should be conducted to confirm the emulsion's corrosion inhibiting abilities in practical settings. Lastly, commercial LM-based TIMs are applied with a surrounding gasket, so the "slippery" nature of the oil-in-LM exterior surface will not be a barrier to application in microelectronics cooling.
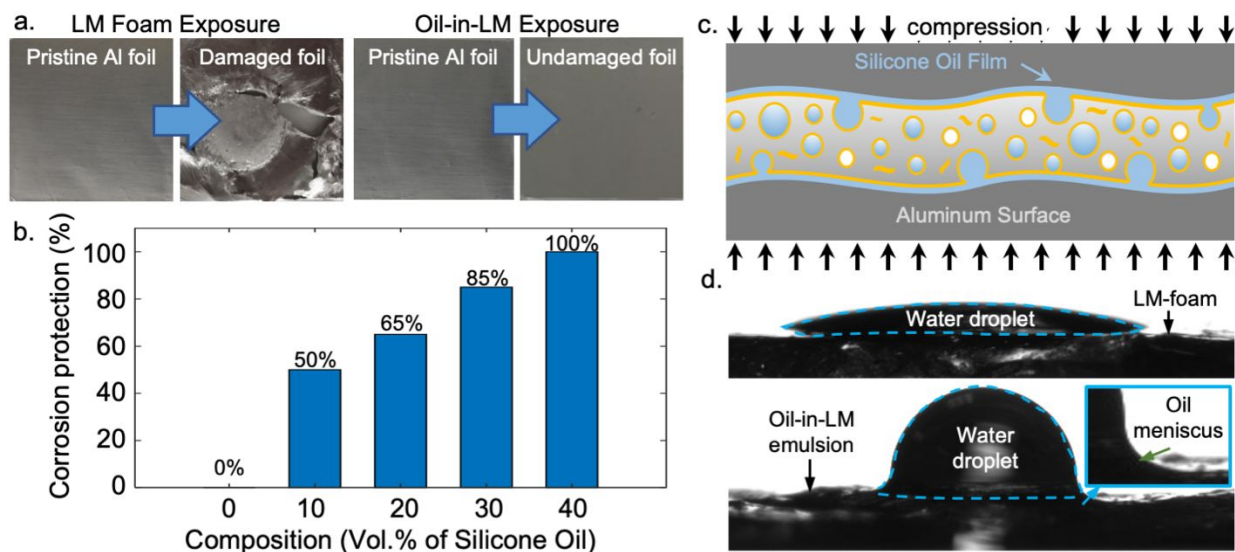
Figure 4. Corrosion protection characteristics of oil-in-LM emulsions (a) representative images of aluminum foil before and after 24-hour contact under 0.1 MPa pressure with LM foam and oil-in-LM emulsion (40:60 SO:LM foam), (b) bar plot showing corrosion protection ability of 10 cSt oil-in-LM emulsions made with varying oil content (total 20 tests were performed for each composition), (c) schematic illustrating the mechanism of aluminum corrosion protection under compression: wetting of the exterior of the emulsions by a thin film of SO, and (d) images of 1 microliter water droplets placed on LM foam and on the 40:60 oil-in-LM emulsion.

Conclusion

In summary, we demonstrated that foam features in LM (oxide flakes, air bubbles, and pores) act as "emulsification agents" that enable the formation of stable oil-in-LM emulsions. Although the emulsions can be created using oils with viscosity ranging from 10 to 10,000 cSt, we revealed that beyond a proper viscosity and mixing time "processing window," the created materials can invert into the more common LM-in-oil emulsions. In particular, the oil-in-LM emulsions made with lower viscosity silicones proved to be resistant to phase inversion up to the tested 120-minute mixing time. We also demonstrated that the use of lower viscosity oils is also beneficial from thermal perspective as it leads to the lowest decrease in the effective thermal conductivity of the

emulsions. The disruption in thermal transport likely stems from oil creating microscale features in addition to the existing foam features (*i.e.*, the oil does not appear to completely displace air in the existing features). As we demonstrated by the increase of the water droplet contact angle from about 10º on LM foam to over 90º on oil-in-LM emulsion, a thin film of the SO coats the exterior of the emulsions. This lubricant-impregnated-surface feature provides a barrier layer between the emulsion and any surfaces that encounters it. We demonstrated that in case of contact with aluminum, the 40:60 SO:LM foam emulsions have sufficient 10 cSt SO barrier layer to entirely prevent the possibility of gallium-induced corrosion of the metal substrate. At this composition, this stable oil-in-LM emulsion has an effective thermal conductivity of 9.5 ± 1.1 Wm^{-1}K^{-1} that is several times higher than currently available TIM greases or pads. As in the case of LMs and their foams, the thermal conductivity of the emulsion can likely be further increased by addition of highly thermally conductive solid particles such as Ag,[50] Cu,[51,52] Fe,[53] Ni,[54,55] W,[42] SiC,[56] and diamond.[57–59] Thus, the oil-in-LM emulsions introduced in this work are a highly promising platform for the next generation of high performance and corrosion-inhibiting TIMs. We expect that the insights gathered from these processing-structure-property relationships of oil-in-LM emulsions will catalyze their further exploration and the use of these new liquid phase composites in other soft applications.

Experimental

Preparation of the LM-in-oil and oil-in-LM emulsions

Gallium (99.99%) was purchased from Rotometals while the silicone oils with viscosity ranging from 10 to 10,000 cSt were obtained from Sigma Aldrich. The LM-in-oil emulsions were

prepared by manually mixing of the pure and melted gallium with the silicone oil in specific volume ratios for various periods of time in a small plastic container using a wooden stir rod. In all cases, this procedure resulted in formation of LM droplets within the oil phase. The oil-in-LM emulsions were prepared in a two-step process: first the stirring of LM in air to create LM foam, followed by mixing of LM foam with oil. In the first step, pure LM was melted and transferred to a plastic beaker in the quantity of 100 g. To prepare the LM foam, the gallium is liquified in a beaker and stirred in air at 600 rpm for two hours using an industrial mixer and a 3D-printed cross-shaped impeller, following our previous work.[33] In the second step, LM foam and silicone oil in specific volume ratios were mixed manually in a small plastic container using a 2.1 mm thick wooden stirring rod. To keep the liquid metal in molten state during all mixing processes, the container was kept on top of a hot plate set at 60 °C.

Sample characterization

We imaged the internal structure of the LM-oil samples using optical and scanning electron microscopy. We prepared the sample cross sections by cleaving the solidified sample blocks (at room temperature) with a razor blade. We collected the electron micrographs with an Amray 1910 FESEM with 15 kV accelerating voltage. In turn, we took the optical images using a Zeiss Axio Zoom.V16 microscope with Apo Z 1.5x/0 37 FWD 30 mm objective. We measured the particle sizes of the LM droplets using Image-J software.

We measured the thermal conductivity of the various emulsions using a steady-state thermal reference bar testing method following a modified ASTM D5470 standard.[39–41,54] We applied the samples onto the copper reference bars and compressed them to a 2.0 mm (±0.2 mm) thickness for each measurement. We used a Teflon gasket to keep the sample in place while testing.

We tested the risk of aluminum corrosion by placing 0.75 g of the LM foam or emulsion in-between two aluminum foil covered glass slides. We applied a steady pressure of 0.1 MPa by placing a weight on top and kept the entire setup on a hot plate at 60 $^\circ$C to keep the samples in a liquid state. We visually inspected the aluminum foils for corrosion after a 1 day or 7-day period. The results are presented as the percentage of the 20 samples that we tested per given data point that were not corroded after contact with the emulsion *(i.e.* 100% protection means that none of the 20 samples was impacted by emulsion contact).

Acknowledgements

References

1   S. Chen, Z. Deng and J. Liu, *Nanotechnology*, 2020, **32**, 092001.

2   S. Chen, H.-Z. Wang, R.-Q. Zhao, W. Rao and J. Liu, *Matter*, 2020, **2**, 1446–1480.

3   C. Majidi, *Matter*, 2021, **4**, 336–337.

4   M. H. Malakooti, M. R. Bockstaller, K. Matyjaszewski and C. Majidi, *Nanoscale Adv.*, 2020, **2**, 2668–2677.

5   S.-Y. Tang, C. Tabor, K. Kalantar-Zadeh and M. D. Dickey, *Annu. Rev. Mater. Res.*, 2021, **51**, 381–408.

6   Y. Lin, J. Genzer and M. D. Dickey, *Adv. Sci.*, 2020, **7**, 2000192.

7   W. Xie, F. M. Allioux, J. Z. Ou, E. Miyako, S. Y. Tang and K. Kalantar-Zadeh, *Trends Biotechnol.*, 2020, **39**, 624–640.

8   C. Wang, Y. Gong, B. V Cunning, S. Lee, Q. Le, S. R. Joshi, O. Buyukcakir, H. Zhang, W. K. Seong, M. Huang, M. Wang, J. Lee, G. Kim and R. S. Ruoff, *Sci. Adv.*, 2021, **7**, eabe3767.

9   T. V. Neumann, E. G. Facchine, B. Leonardo, S. Khan and M. D. Dickey, *Soft Matter*, 2020, **16**, 6608–6618.

10   K. M. Razeeb, E. Dalton, G. L. W. Cross and A. J. Robinson, *Int. Mater. Rev.*, 2018, **63**, 1–21.

11   R. Prasher, *Proc. IEEE*, 2006, **94**, 1571–1586.

12   C. P. Feng, L. Y. Yang, J. Yang, L. Bai, R. Y. Bao, Z. Y. Liu, M. B. Yang, H. B. Lan and W. Yang, *Compos. Commun.*, 2020, **22**, 100528.

13   R. N. Lyon, *Liquid Metals Handbook, The Committee on the Basic Properties of Liquid Metals*, 1952.

14   M. Rajagopalan, M. A. Bhatia, M. A. Tschopp, D. J. Srolovitz and K. N. Solanki, *Acta Mater.*, 2014, **73**, 312–325.

15   S. G. Keller and A. P. Gordon, *Eng. Fract. Mech.*, 2012, **84**, 146–160.

16   X. Wang and J. Liu, *Micromachines*, 2016, **7**, 206.

17   A. Ndieguene, P. Albert and J. Sylvestre, in *Electronic Components and Technology Conference (ECTC), 2016 IEEE 66th*, IEEE, 2016, pp. 580–587.

18   R. McAfee, M. Fish, D. Baker, J. Gess and L. Boteler, in *2020 19th IEEE Intersociety Conference on Thermal and Thermomechanical Phenomena in Electronic Systems (ITherm)*, IEEE, 2020, pp. 1276–1281.

19   T. Hellebrekers, K. B. Ozutemiz, J. Yin and C. Majidi, in *2018 IEEE/RSJ International Conference on Intelligent Robots and Systems (IROS)*, IEEE, 2018, pp. 5924–5929.

20   K. B. Ozutemiz, J. Wissman, O. B. Ozdoganlar and C. Majidi, *Adv. Mater. Interfaces*, 2018, **5**, 1701596.

21   N. Kazem, T. Hellebrekers and C. Majidi, *Adv. Mater.*, 2017, **29**, 1605985.

22   R. W. Style, R. Tutika, J. Y. Kim and M. D. Bartlett, *Adv. Funct. Mater.*, 2020, **31**, 2005804.

23   P. Fan, Z. Sun, Y. Wang, H. Chang, P. Zhang, S. Yao, C. Lu, W. Rao and J. Liu, *RSC Adv.*, 2018, **8**, 16232–16242.

24   M. D. Bartlett, N. Kazem, M. J. Powell-Palm, X. Huang, W. Sun, J. A. Malen and C. Majidi, *Proc. Natl. Acad. Sci.*, 2017, **114**, 2143–2148.

25   S. Mei, Y. Gao, Z. Deng and J. Liu, *J. Electron. Packag.*, 2014, **136**, 011009.

26   Q. Xu, N. Oudalov, Q. Guo, H. M. Jaeger and E. Brown, *Phys. Fluids*, 2012, **24**, 1–13.

27   A. Perazzo, V. Preziosi and S. Guido, *Adv. Colloid Interface Sci.*, 2015, **222**, 581–599.

28   A. Kumar, S. Li, C. M. Cheng and D. Lee, *Ind. Eng. Chem. Res.*, 2015, **54**, 8375–8396.

29   Y. Liu, W. Zhang and H. Wang, *Mater. Horizons*, 2020, **8**, 56–77.

30   M. R. Khan, C. B. Eaker, E. F. Bowden and M. D. Dickey, *Proc. Natl. Acad. Sci.*, 2014, **111**, 14047–14051.

31   C. B. Eaker, D. C. Hight, J. D. O'Regan, M. D. Dickey and K. E. Daniels, *Phys. Rev. Lett.*, 2017, **119**, 174502.

32   X. Wang, L. Fan, J. Zhang, X. Sun, H. Chang, B. Yuan, R. Guo, M. Duan and J. Liu, *Adv. Funct. Mater.*, 2019, 1907063.

33   W. Kong, N. U. H. Shah, T. V Neumann, M. H. Vong, P. Kotagama, M. D. Dickey, R. Y.

Wang and K. Rykaczewski, *Soft Matter*, 2020, **16**, 5801–5805.

34   M. Zhang, L. Liu, C. Zhang, H. Chang, P. Zhang and W. Rao, *Adv. Mater. Interfaces*, 2021, 2100432.

35   J. Gao, J. Ye, S. Chen, J. Gong, Q. Wang and J. Liu, *ACS Appl. Mater. Interfaces*, 2021, **13**, 17093–17103.

36   H. Wang, B. Yuan, S. Liang, R. Guo, W. Rao, X. Wang, H. Chang, Y. Ding, J. Liu and L. Wang, *Mater. Horizons*, 2018, **5**, 222–229.

37   R. Tutika, S. Kmiec, A. B. M. T. Haque, S. W. Martin and M. D. Bartlett, *ACS Appl. Mater. Interfaces*, 2019, **11**, 17873–17883.

38   A. Koh, J. Sietins, G. Slipher and R. Mrozek, *J. Mater. Res.*, 2018, **33**, 2443–2453.

39   M. I. M. I. Ralphs, N. Kemme, P. B. P. B. Vartak, E. Joseph, S. Tipnis, S. Turnage, K. N. Solanki, R. Y. R. Y. R. Y. Wang and K. Rykaczewski, *ACS Appl. Mater. Interfaces*, 2018, **10**, 2083–2092.

40   D. R. Thompson, S. R. Rao and B. A. Cola, *J. Electron. Packag.*, 2013, **135**, 41002.

41   R. Kempers, P. Kolodner, A. Lyons and A. J. Robinson, *Rev. Sci. Instrum.*, 2009, **80**, 1–11.

42   W. Kong, Z. Wang, M. Wang, K. C. Manning, A. Uppal, M. D. Green, R. Y. Wang and K. Rykaczewski, *Adv. Mater.*, 2019, **31**, 1904309.

43   H. Fukuyama, T. Yoshimura, H. Yasuda and H. Ohta, *Int. J. Thermophys.*, 2006, **27**, 1760–1777.

44   S. Anand, K. Rykaczewski, S. B. Subramanyam, D. Beysens and K. K. Varanasi, *Soft Matter*, 2015, **11**, 69–80.

45   V. G. Damle, A. Tummala, S. Chandrashekar, C. Kido, A. Roopesh, X. Sun, K. Doudrick,

J. Chinn, J. R. Lee, T. P. Burgin and K. Rykaczewski, *ACS Appl. Mater. Interfaces*, 2015, **7**, 4224–4232.

46   J. D. Smith, R. Dhiman, S. Anand, E. Reza-Garduno, R. E. Cohen, G. H. McKinley and K. K. Varanasi, *Soft Matter*, 2013, **9**, 1772–1780.

47   J. B. Boreyko, G. Polizos, P. G. Datskos, S. A. Sarles and C. P. Collier, *Proc. Natl. Acad. Sci.*, 2014, **111**, 7588–7593.

48   R. Qiu, Q. Zhang, P. Wang, L. Jiang, J. Hou, W. Guo and H. Zhang, *Colloids Surfaces A Physicochem. Eng. Asp.*, 2014, **453**, 132–141.

49   P. Wang, Z. Lu and D. Zhang, *Corros. Sci.*, 2015, **93**, 159–166.

50   Z. Lin, H. Liu, Q. Li, H. Liu, S. Chu, Y. Yang and G. Chu, *Appl. Phys. A*, 2018, **124**, 368.

51   J. Tang, X. Zhao, J. Li, R. Guo, Y. Zhou and J. Liu, *ACS Appl. Mater. Interfaces*, 2017, **9**, 35977–35987.

52   S. Ki, J. Shim, S. Oh, E. Koh, D. Seo, S. Ryu, J. Kim and Y. Nam, *Int. J. Heat Mass Transf.*, 2021, **170**, 121012.

53   L. Hu, H. Wang, X. Wang, X. Liu, J. Guo and J. Liu, *ACS Appl. Mater. Interfaces*, 2019, **11**, 8685–8692.

54   M. Ralphs, W. Kong, R. Y. R. Y. Wang and K. Rykaczewski, *Adv. Mater. Interfaces*, 2019, **6**, 1801857.

55   U. Daalkhaijav, O. D. Yirmibesoglu, S. Walker and Y. Mengüç, *Adv. Mater. Technol.*, 2018, **3**, 1700351.

56   W. Kong, Z. Wang, N. Casey, M. M. Korah, A. Uppal, M. D. Green, K. Rykaczewski and R. Y. Wang, *Adv. Mater. Interfaces*, 2021, 2100069.

57   S. Wei, L. Zhou and J. Guo, *2018 19th Int. Conf. Electron. Packaing Technol.*, 2018,

1333–1336.

58   S. W. Z. F. Yu and L. J. Z. J. D. Guo, *J. Mater. Sci. Mater. Electron.*, 2019, **30**, 7194–

        7202.

59   C. Zeng, J. Shen and J. Zhang, *Diam. Relat. Mater.*, 2021, **112**, 108230.